eTransportation 16 (2023) 100225

Contents lists available at ScienceDirect

eTransportation

journal homepage: www.journals.elsevier.com/etransportation

Techno-economic cell selection for battery-electric long-haul trucks

Olaf Teichert [a,*], Steffen Link [b], Jakob Schneider [a], Sebastian Wolff [a], Markus Lienkamp [a]

[a] Technical University of Munich, School of Engineering & Design, Institute of Automotive Technology, 85748 Garching, Germany
[b] Fraunhofer Institute for Systems and Innovation Research ISI, 76139 Karlsruhe, Germany

ARTICLE INFO

Keywords:
Techno-economic design
Battery cell selection
Lithium-ion
Battery-electric trucks

ABSTRACT

To reach cost-parity with diesel trucks, battery-electric trucks require fast-chargeable lithium-ion cells with a high energy density and cycle life, at a low specific cost. However, cells generally excel at only a fraction of these characteristics. To help select the optimal cell, we have developed the techno-economic cell selection method. The method determines the price per kilowatt-hour that is required to reach cost-parity with a diesel truck, based on the characteristics provided in a cell's datasheet. We demonstrate the method by selecting the optimal cell out of a database containing 160 cells for a long-haul truck operating with a single driver in Germany in two scenarios: charged at 350 kW and charged at 1 MW. The results show that for trucks charged at the current maximum charging power of 350 kW, the cell price needs to drop to ca. €60 kW^{-1} h to reach cost-parity with a diesel truck. When 1 MW charging power is available, cost-parity can be reached at a cell price around €100 kW^{-1} h, which is within reach of optimistic cost estimates. However, the most cost-effective cells require more volume and result in a lower maximum payload than a diesel truck. A parameter sensitivity analysis shows that best-in-class cell energy density and packaging efficiency are required to match the payload capacity and powertrain volume of a diesel truck. The cell cycle life, cost of charging and vehicle energy consumption have the biggest impact on the cost-effectiveness of battery electric trucks.

1. Introduction

Heavy-duty vehicles generate a quarter of all green house gas emissions in the transport sector, meaning that they must be quickly decarbonized if climate targets are to be met [1]. One option for reducing emissions is the implementation of battery-electric trucks (BET), which has been the subject of a wide range of studies and reports [2]. Whether BETs become cost-competitive with diesel trucks (DT) depends on the vehicle-acquisition cost, fuel and electricity prices [3], available charging infrastructure [4], driving distance [5] and local policy [6]. Furthermore, the battery of a BET must be: light, to avoid any reductions in payload; small, to fit into the available volume on board the vehicle; fast-charging capable, to enable recharging during driver rest periods; resistant to aging, to avoid battery replacement during the service life; and low-cost to minimize investment costs. Previous studies have investigated the suitability of different cell technologies for BETs.

Sripad et al. [7] carried out Monte-Carlo simulations to determine the required battery capacity and resulting battery weight, battery cost, and maximum payload capacity, for status-quo lithium-ion cells and beyond-lithium-ion cells. Their results show that in order to achieve cost-competitiveness with DTs the improved performance of beyond-lithium-ion cells is required. However, these results might be overly conservative because the authors did not consider en-route fast-charging.

Mareev et al. [8] determined the required battery capacity for long-haul truck operation in Germany incorporating battery charging during driver rest periods. Subsequently they conducted a life cycle cost analysis for a low-cost low-performance cell and a high-cost high-performance cell. Their results show that the life cycle costs are strongly influenced by the battery life, justifying the use of more expensive, but aging-resistant cells.

Çabukoglu et al. [9] investigated the feasibility of BETs in a case study in Switzerland, showing that the share of vehicle kilometers that can be electrified increases when the energy density of the batteries is increased.

Nykvist and Olsson [10] modeled the feasibility of BETs that use high-power fast charging. Their results show that the battery properties strongly influence the cost-competitiveness of BETs and that battery life may be more important than the specific battery price.

Mauler et al. [11] compared the life cycle costs of a BET with lithium iron phosphate (LFP) cells, a BET with high-nickel cells and a hydrogen truck in the US, taking into account the profits foregone due to charging times and lower cargo capacity. Their results

* Corresponding author.
E-mail address: olaf.teichert@tum.de (O. Teichert).

https://doi.org/10.1016/j.etran.2022.100225
Received 12 May 2022; Received in revised form 28 October 2022; Accepted 26 December 2022
Available online 30 December 2022

Nomenclature

Vehicle simulation

a	Applied acceleration in $\mathrm{m\,s^{-2}}$
a_{acc}	Acceleration limit in $\mathrm{m\,s^{-2}}$
a_{dec}	Deceleration limit in $\mathrm{m\,s^{-2}}$
a_{mot}	Max. acceleration achievable by motor in $\mathrm{m\,s^{-2}}$
a_{target}	Target acceleration in $\mathrm{m\,s^{-2}}$
b	Energy consumption in $\mathrm{kW\,h\,km^{-1}}$
c_{A}	Drag area in $\mathrm{m^2}$
c_{rr}	Coefficient of rolling resistance
$f_{\mathrm{b}}(m)$	Interpolant: energy consumption vs. vehicle mass
$f_{\mathrm{v}}(m)$	Interpolant: avg. speed vs. vehicle mass
F_{drag}	Drag resistance in N
F_{incl}	Inclination resistance in N
F_{res}	Total driving resistance in N
F_{roll}	Rolling resistance in N
g	Gravitational acceleration in $\mathrm{m\,s^{-2}}$
j	Simulation step index
k	Driving cycle step index
k_{dec}	Index where a target speed reduction occurs
m	Vehicle mass in kg
P	Applied motor power in W
P_{aux}	Auxiliary power consumption in W
P_{bat}	Battery power in W
P_{mot}	Rated motor power in W
s	Distance along the route in m
t	Time in s
t_{stop}	Stop duration in s
v	Vehicle speed in $\mathrm{m\,s^{-1}}$
v_{cycle}	Target speed defined by driving cycle in $\mathrm{m\,s^{-1}}$
v_{target}	Target speed incl. deceleration phases in $\mathrm{m\,s^{-1}}$
α	Slope in radians
Δs	Distance step length in m
η	Powertrain efficiency
ρ	Air density in $\mathrm{kg\,m^{-3}}$

Battery sizing

b_{BET}	Typical BET energy consumption in $\mathrm{kW\,h\,km^{-1}}$
E_{bat}	Required battery size in kWh
$E_{\mathrm{crate\text{-}lim}}$	Required battery size for cell charging rate in kWh
E_{Plim}	Required battery size for charging power in kWh
E_{max}	Energy demand without fast charging in kWh
m_{bat}	Battery mass in kg
m_{gvw}	Gross vehicle weight in t
$m_{\mathrm{payload,max}}$	Maximum payload in kg
m_{spec}	Cell specific energy in $\mathrm{Wh\,kg^{-1}}$
$m_{\mathrm{veh,nobat}}$	Vehicle mass without battery in t
n_{cycle}	Cell cycle life
s_{life}	Battery life in km
V_{bat}	Battery volume in L
z_{fc}	Share of fast chargeable energy
z_{EOL}	Share of energy at battery replacement
$z_{\mathrm{m,c2s}}$	Gravimetric packaging efficiency
$z_{\mathrm{V,c2s}}$	Volumetric packaging efficiency
ρ_{cell}	Cell energy density in $\mathrm{Wh\,L^{-1}}$

Cost model

b_{DT}	Typical DT energy consumption in $\mathrm{L\,km^{-1}}$
C_{bat}	Battery cost in €
$C_{\mathrm{bat,inv}}$	Battery investment in €
$C_{\mathrm{bat,scrap}}$	Battery scrappage value in €
$C_{\mathrm{bat,res}}$	Battery residual value in €
$C_{\mathrm{bat,imp}}$	Battery imputed interest in €
c_{diesel}	Diesel cost in $€\,\mathrm{L^{-1}}$
c_{ene}	Specific energy cost in $€\,\mathrm{km^{-1}}$
C_{ene}	Energy costs in €
c_{fc}	Cost of fast charging in $€\,\mathrm{kW^{-1}\,h}$
c_{maint}	Specific maintenance cost in $€\,\mathrm{km^{-1}}$
C_{maint}	Maintenance costs in €
C_{pt}	Powertrain cost in €
$C_{\mathrm{pt,inv}}$	Powertrain investment €
$C_{\mathrm{pt,res}}$	Powertrain residual value in €
$C_{\mathrm{pt,imp}}$	Powertrain imputed interest in €
c_{sc}	Cost of slow charging in $€\,\mathrm{kW^{-1}\,h}$
c_{spec}	Cell specific cost in $€\,\mathrm{kW^{-1}\,h}$
c_{tax}	Annual motor vehicle tax in $€\,\mathrm{years^{-1}}$
C_{taxes}	Taxes in €
c_{toll}	Toll cost in $€\,\mathrm{km^{-1}}$
C_{tolls}	Tolls in €
n_{repl}	Number of battery replacements
r	Discount rate
s_{annual}	Annual vehicle mileage in km
t_{own}	Ownership duration in years
$z_{\mathrm{c,c2s}}$	Ratio between cell and system costs
$z_{\mathrm{ene,fc}}$	Share of fast charged energy
z_{scr}	Ratio between investment and scrappage value
z_{SOH}	Share of remaining battery life
z_{toll}	Share of kilometers driven on toll roads

show that LFP batteries excel in volume-constrained transport on short routes, whereas high-nickel batteries have the advantage in weight-constrained transportation. Hydrogen trucks only become cost-competitive on routes that are long and weight-constrained.

Although these studies recognize the impact of the battery cell properties, a method for selecting the optimal cell is still missing. Other studies have developed methods for cell selection in general.

The most well-known decision aid for energy storage device selection is the Ragone plot presented by David Ragone in 1968 [12]. The Ragone plot maps energy density and power density to automotive driving requirements, such as top speed and range, enabling the selection of a suitable energy storage device. Since its introduction, the Ragone plot has been extended to include a wider variety of energy storage technologies, such as supercapacitors or lithium-ion batteries, and has been applied in a wider range of applications [13].

More recently, Catenaro et al. [14] developed an enhanced Ragone plot that takes the operating temperature of the cell into account. Dechent et al. [15] proposed a further extension of the Ragone plot, called ENPOLITE, which visualizes the energy, power, lifetime and temperature of energy storage technologies in a single figure.

Although these cell selection methods visualize the characteristics of a wide range of energy storage technologies, they do not quantify the impact of the cell selection on the system costs. On the other hand, life cycle cost studies only compare a small number of cell technologies and do not provide a tool for selecting the best cell from a database.

To bridge this gap, we have developed the techno-economic cell selection method for BETs to support selecting the optimal individual cell. The method uses the characteristics specified in a cell's datasheet to determine the price per kWh required to reach cost-parity with a DT, in the following referred to as the cost-parity price. We demonstrate the method by selecting the optimal cell from a database containing 160 cells for a long-haul BET operating with a single driver in Germany.

The contributions of this study can be summarized as follows:

- a novel cell selection method that incorporates the trade-off between cell cost and performance;
- results showing the cost-competitiveness of different cell chemistries and cell formats for a BET application;
- a parameter sensitivity analysis quantifies the impact of cell, pack, and system characteristics.

The method serves as a decision making aid for battery designers at truck manufacturing companies. Furthermore, the method can be used by cell manufacturers to optimize their cell design. The method and the developed cell database are available open source and can be accessed at the following repository: https://github.com/TUMFTM/TechnoEconomicCellSelection.

2. Method

To determine the cost-parity price for a single cell, we combine a vehicle simulation with a battery sizing algorithm and a cost model, as illustrated in Fig. 1. First, the vehicle simulation determines the energy consumption and average speed for a range of vehicle masses, based on the vehicle parameters and a driving cycle. The results are used to create interpolation functions between vehicle mass on the one hand, and energy consumption and average speed on the other. Second, the battery sizing algorithm determines the required battery size subject to the results from the vehicle simulation, cell properties and mobility requirements. The volume, weight, maximum payload, typical energy consumption and battery life are calculated for the determined battery size. Third, based on the results from the battery sizing algorithm and cost & operating conditions, the cost model determines the cost-parity price, using bisection to minimize the cost difference between a BET and a DT.

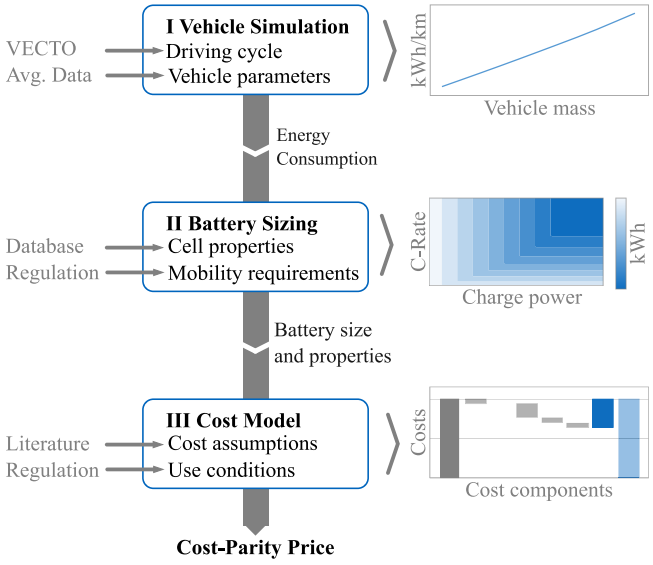

Fig. 1. Schematic representation of the techno-economic cell selection for BET, which combines a vehicle simulation with a battery sizing algorithm and a cost model.

2.1. Vehicle simulation

The vehicle model simulates a vehicle's speed and energy consumption using a quasi-static distance-based longitudinal-dynamics model, based on the vehicle characteristics and the VECTO long-haul driving cycle [16]. The driving cycle defines the target speed, road gradient and duration of stops along a route, as shown in Fig. 2.

The driving cycle does not prescribe braking or acceleration behavior because these are strongly influenced by the vehicle characteristics. The acceleration and braking behavior are therefore determined by the simulation. We simulate braking behavior by adding constant deceleration phases in front of distance steps at which a reduction of the target speed occurs, in accordance with Eq. (1), where $v_{\mathrm{target,k}}$ denotes the modified target speed at a distance step with index k, v_{cycle} is the driving cycle target speed, $\mathrm{k_{dec}}$ is the distance step index at which the target speed reduction occurs, a_{dec} is the deceleration, and s_{k} is the distance along the route. Fig. 3 illustrates the addition of a deceleration phase.

$$v_{\mathrm{target,k}} = \sqrt{v^2_{\mathrm{cycle,k=k_{dec}}} + 2\ a_{\mathrm{dec}}\ (s_{\mathrm{k=k_{dec}}} - s_{\mathrm{k}})} \tag{1}$$

The acceleration behavior and energy consumption of the truck are then simulated in a forward simulation. The simulation uses a different step index, denoted j, because two time-values occur for a single distance-value during a stop. The start conditions are given by Eq. (2), where t denotes the time and v the vehicle speed.

$$\begin{aligned} s_{\mathrm{j=1}} &= 0 \\ t_{\mathrm{j=1}} &= 0 \\ v_{\mathrm{j=1}} &= 0 \end{aligned} \tag{2}$$

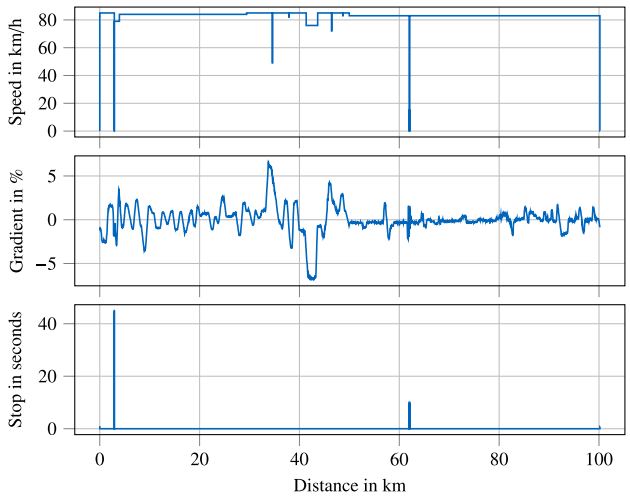

Fig. 2. The VECTO long-haul driving cycle is one of a range of driving cycles that was developed by the European commission to determine the CO_2 emissions from heavy-duty vehicles and represents the typical operation of a long-haul truck [16].

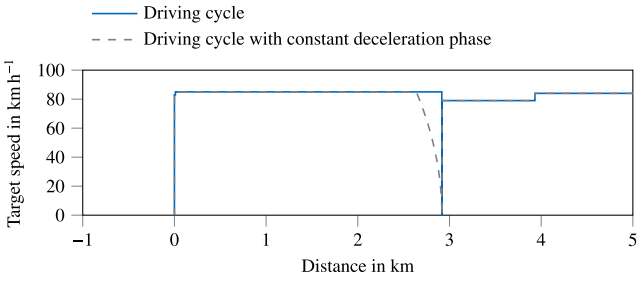

Fig. 3. Illustration of an added constant deceleration phase.

For every distance step, we first check if the vehicle is stopped. If it is, an additional data point is added according to Eq. (3), where t_{stop} denotes the stop duration and P the applied motor power.

$$\left.\begin{aligned} s_{j+1} &= s_j \\ t_{j+1} &= t_j + t_{stop,k} \\ v_{j+1} &= 0 \\ P_j &= 0 \\ j &= j+1 \end{aligned}\right\} \text{if } t_{stop,k} > 0 \tag{3}$$

Subsequently, the driving resistances are calculated using Eqs. (4)–(6), where m denotes the vehicle mass, g the gravitational acceleration, c_{rr} the rolling resistance coefficient, α the slope, ρ the density of air, and c_A the drag area.

$$F_{roll,j} = m\ g\ c_{rr} \cos(\alpha_k) \tag{4}$$

$$F_{drag,j} = 0.5\ \rho\ c_A\ v_j^2 \tag{5}$$

$$F_{incl,j} = m\ g \sin(\alpha_k) \tag{6}$$

Then we calculate the acceleration required to reach the target speed, a_{target}, and the maximum acceleration that can be achieved by the motor, a_{mot}, using Eqs. (7) and (8), respectively, where Δs denotes the distance step length, P_{mot} the rated motor power, and η the overall powertrain efficiency,

$$a_{target,j} = \frac{v_{target,k+1}^2 - v_j^2}{2\ \Delta s} \tag{7}$$

$$a_{mot,j} = \frac{1}{m}\left(\frac{P_{mot}\ \eta}{v_j} - F_{roll,j} - F_{incl,j} - F_{drag,j}\right) \tag{8}$$

The applied acceleration is the minimum of the target acceleration, motor-limited acceleration and an absolute acceleration limit, $a_{acc,max}$, as shown in Eq. (9).

$$a_j = \min(a_{target,j}, a_{mot,j}, a_{acc,max}) \tag{9}$$

Based on the applied acceleration, the new vehicle speed, time, and applied power are calculated using Eq. (10)–(14).

$$v_{j+1} = \sqrt{v_j^2 + 2\ a_j \Delta s} \tag{10}$$

$$t_{j+1} = t_j + \frac{2\ \Delta s}{v_j + v_{j+1}} \tag{11}$$

$$s_{j+1} = s_j + \Delta s \tag{12}$$

$$F_{res,j} = m\ a_j + F_{roll,j} + F_{drag,j} + F_{incl,j} \tag{13}$$

$$P_j = F_{res,j}\ v_j\ \eta^{-\mathrm{sgn}(F_{res,j})} \tag{14}$$

Finally, we calculate the power drawn from or supplied to the battery using Eq. (15), where we assume that negative powers up to the rated motor power are recuperated and the remaining power is converted into heat by the mechanical brakes.

$$P_{bat,j} = \max(P_j, -P_{mot}) \tag{15}$$

Eq. (3) to (15) are repeated for every distance step in the driving cycle. The energy consumption per kilometer can then be calculated using Eq. (16), where P_{aux} denotes the energy consumption of auxiliary loads and n is the number of simulation steps. The constant corresponds to the conversion from $\mathrm{kJ\,km^{-1}}$ to $\mathrm{kW\,h\,km^{-1}}$.

$$b = \frac{1}{3600\ s_{j=n}}\left(P_{aux}\ t_{j=n} + \sum_{j=1}^{j=n-1} P_{bat,j}(t_{j+1} - t_j)\right) \tag{16}$$

The average vehicle speed v_{avg} is calculated using Eq. (17), where the constant corresponds to the conversion from $\mathrm{m\,s^{-1}}$ to $\mathrm{km\,h^{-1}}$.

$$v_{avg} = 3.6\frac{s_{j=n}}{t_{j=n}} \tag{17}$$

The vehicle simulation is executed for a range of vehicle weights to generate the linear interpolation functions $f_b(m)$ and $f_v(m)$ for energy consumption and average speed, respectively.

2.2. Battery sizing model

The battery sizing algorithm determines the required battery size subject to the results from the vehicle simulation, cell properties and mobility requirements. The BET mimics the operation of a DT without any additional time loss.

In Europe, truck drivers are prohibited to drive for more than 4.5 h at a time and are then required to take a 45 minute break before continuing [17]. The 45 minute break may be replaced by a break of at least 15 minutes followed by a break of at least 30 min, which would result in the same rest duration after 4.5 h of driving. We assume that these rest periods can be used to recharge the BET. The daily driving time is limited to 10 h [17]. For a 10-hour drive, the battery can be recharged before the last hour of driving, which makes a 9-hour drive with a 45 minute break the most demanding single-driver scenario in Europe.

The maximum energy demand for driving nine hours, E_{max} is given by Eq. (18), where m_{gvw} is the gross vehicle weight, i.e. the maximum combined operating weight of the truck, trailer and payload.

$$E_{max} = 9\ f_b(m_{gvw})\ f_v(m_{gvw}) \tag{18}$$

The battery size that is required to complete a day of driving depends on the amount of energy that can be recharged during the rest period, as illustrated in Appendix A. The amount of energy that can be recharged during the rest period may be limited by the installed charging power, given by Eq. (19), or the cell's charging rate, given by Eq. (20). P_{fc} denotes the installed charging power, t_{fc} the time available for charging, z_{EOL} the share of remaining energy at battery replacement, z_{usable} the share of usable energy, C_{cell} the cell's charging rate, and z_{fc} the share of the battery that can be recharged using fast charging. The required battery size is simply the maximum of both constraints, Eq. (21). Note that the resulting battery can power a fully loaded vehicle for the maximal legal driving duration during its entire operating life.

$$E_{P\text{-}lim} = E_{max} - P_{fc}\ t_{fc} \tag{19}$$

$$E_{crate\text{-}lim} = \frac{E_{max}}{1 + \min(\frac{C_{cell}\ t_{fc}}{z_{EOL}\ z_{usable}}, z_{fc})} \tag{20}$$

$$E_{bat} = \frac{\max(E_{crate\text{-}lim}, E_{P\text{-}lim})}{z_{EOL}\ z_{usable}} \tag{21}$$

Based on the determined battery size, the battery volume, V_{bat}, battery weight, m_{bat}, and the resulting maximum payload, $m_{payload,max}$, can be calculated using Eq. (22)–(24), where ρ_{cell} and m_{spec} denote a cell's energy density and specific energy, $z_{m,c2s}$ and $z_{V,c2s}$ the gravimetric and volumetric packaging efficiency, and $m_{veh,nobat}$ the weight of the vehicle without the battery.

$$V_{bat} = \frac{E_{bat}}{\rho_{cell}\ z_{V,c2s}} \tag{22}$$

$$m_{bat} = \frac{E_{bat}}{m_{spec}\ z_{m,c2s}} \tag{23}$$

$$m_{payload,max} = m_{gvw} - m_{veh,nobat} - m_{bat} \tag{24}$$

Eq. (25) then calculates the typical energy consumption, b_{BET}, under the loading conditions that are used by the European Commission to estimate the CO_2 emissions during long-haul operation of a newly registered truck. These correspond to a low load of 2.6 t over 30 % of the trip distance and a reference load of 19.3 t over the remaining 70 % [18]. A cell resulting in a maximum payload below the reference load is considered unfeasible for a long-haul BET.

$$\begin{aligned} b_{BET} =& 0.3 f_{con}(m_{bat} + m_{veh,nobat} + 2600) \\ &+ 0.7 f_{con}(m_{bat} + m_{veh,nobat} + 19300) \end{aligned} \tag{25}$$

Finally, the battery life in kilometers, s_{life}, is calculated using Eq. (26), where n_{cycle} denotes the cell's cycle life.

$$s_{life} = \frac{E_{bat}\ n_{cycle}}{b_{BET}} \tag{26}$$

2.3. Cost model

To determine cost-parity, the cost model only needs to consider the cost components that differ between a BET and a DT. To determine these cost-components, a cost breakdown of a long-haul truck was analyzed, shown in Table 1. Converting a DT to a BET affects the cost of the powertrain (motor and transmission) and battery, but is assumed not to influence the cost of other vehicle components. Additionally, the conversion influences the maintenance costs, cost of energy, taxes and tolls. The costs for insurance and the driver are assumed to be unaffected because the vehicle operation remains unchanged. BET subsidies are not considered.

The sum of cost components that differ between a BET and a DT is referred to as the relevant cost of ownership (RCO) and is given by Eq. (27), where C_{maint} denotes the maintenance costs, C_{ene} the cost for energy consumption, C_{taxes} taxes, C_{tolls} tolls, C_{pt} the powertrain costs, and C_{bat} the battery costs. To account for both operating costs and investment costs, all costs are expressed by their net present value.

$$\text{RCO} = C_{\text{maint}} + C_{\text{ene}} + C_{\text{taxes}} + C_{\text{tolls}} + C_{\text{pt}} + C_{\text{bat}} \tag{27}$$

We assume that taxes are due annually, maintenance costs are incurred twice a year, and toll and energy are paid weekly. The corresponding net present value is then calculated using Eq. (28) to (31), where t_{own} denotes the ownership duration in years, r the discount rate, c_{tax} the annual motor vehicle tax, s_{annual} the annual vehicle mileage, c_{maint} the specific maintenance cost per kilometer, z_{toll} the share of kilometers driven on toll roads, c_{toll} the toll costs per kilometer, and c_{ene} the cost of energy per kilometer. The cost of energy for diesel trucks simply corresponds to the product of the DT consumption, b_{DT}, and the cost of diesel per liter, c_{diesel}. The cost of energy for the BET is the product of the typical BET consumption, b_{BET}, and the cost of charging, which differentiates between slow charging overnight, c_{sc}, and fast charging, c_{fc}, where $z_{\text{ene,fc}}$ denotes the share of fast charged energy. To avoid any bias from forecasts, we assume that the electricity costs and diesel costs are constant throughout the ownership duration.

$$C_{\text{taxes}} = \sum_{n=1}^{n=t_{\text{own}}} c_{\text{tax}} r^{-n} \tag{28}$$

$$C_{\text{maint}} = \sum_{n=0}^{n=2\times t_{\text{own}}-1} \frac{1}{2}\, s_{\text{annual}} c_{\text{maint}}\, r^{-n/2} \tag{29}$$

$$C_{\text{toll}} = \sum_{n=0}^{n=52\times t_{\text{own}}-1} \frac{1}{52}\, s_{\text{annual}}\, z_{\text{toll}} c_{\text{toll}}\, r^{-n/52} \tag{30}$$

$$C_{\text{ene}} = \sum_{n=0}^{n=52\times t_{\text{own}}-1} \frac{1}{52} s_{\text{annual}} c_{\text{ene}}\, r^{-n/52} \tag{31}$$

$$\text{where}\quad c_{\text{ene}} = \begin{cases} b_{\text{DT}}\, c_{\text{diesel}} & \text{for DT} \\ b_{\text{BET}} \left(c_{\text{fc}}\, z_{\text{ene,fc}} + c_{\text{sc}}\, (1 - z_{\text{ene,fc}}) \right) & \text{for BET} \end{cases}$$

The powertrain costs include the initial investment, $c_{\text{pt,inv}}$, the resale value at the end of ownership, $c_{\text{pt,res}}$, and the imputed interest, $c_{\text{pt,imp}}$, given by (32). The resale value is calculated by Eq. (33), where the first term in the equation describes the relation between the resale value and the vehicle mileage that was determined for a semi-trailer truck by Kleiner and Friedrich [19]. The imputed interest describes the interest that could have been earned by the bound investment and is given by Eq. (34).

$$C_{\text{pt}} = C_{\text{pt,inv}} - C_{\text{pt,res}} + C_{\text{pt,imp}} \tag{32}$$

$$C_{\text{pt,res}} = (0.951 \exp(\frac{-t_{\text{own}} s_{\text{annual}}}{500000}))\; C_{\text{pt,inv}}\; r^{-t_{\text{own}}} \tag{33}$$

$$C_{\text{pt,imp}} = \frac{C_{\text{pt,inv}} + C_{\text{pt,res}}}{2} (r^{t_{\text{own}}} - 1) \tag{34}$$

The RCO of diesel trucks does not include any battery costs. For the BET, the costs for the battery consist of the sum of all investments, $C_{\text{bat,inv}}$, the scrappage value of all replaced batteries (e.g. for use in second-life applications), $C_{\text{bat,scrap}}$, the resale value at the end of ownership $C_{\text{bat,res}}$ and the imputed interest, $C_{\text{bat,imp}}$, as given in Eq. (35).

$$C_{\text{bat}} = \sum C_{\text{bat,inv,n}} - \sum C_{\text{bat,scrap,n}} - C_{\text{bat,res}} + C_{\text{bat,imp}} \tag{35}$$

The investment costs are given by Eq. (36), where c_{spec} denotes the specific battery costs and $z_{\text{c,c2s}}$ the ratio between costs at the cell and system level. The number of required replacements, n_{repl}, is given by Eq. (37).

$$C_{\text{bat,inv,n}} = c_{\text{spec}} z_{\text{c,c2s}}\; E_{\text{bat}}\; r^{-\frac{n\; s_{\text{life}}}{s_{\text{annual}}}} \quad \forall\; n \in [0, \ldots, n_{\text{repl}}] \tag{36}$$

$$n_{\text{repl}} = \lfloor t_{\text{own}} s_{\text{annual}} / s_{\text{life}} \rfloor \tag{37}$$

The value for second-use applications is calculated with Eq. (38), where z_{scr} denotes the share of remaining value at scrappage.

$$C_{\text{bat,scrap,n}} = z_{\text{scr}} c_{\text{spec}}\; z_{\text{c,c2s}}\; E_{\text{bat}}\; r^{-\frac{n\; s_{\text{life}}}{s_{\text{annual}}}} \quad \forall\; n \in [1, \ldots, n_{\text{repl}}] \tag{38}$$

The resale value of the battery at the end of ownership is assumed to be proportional to the remaining battery life as given by Eq. (39), where the remaining battery life, z_{SOH}, is calculated from Eq. (40). Finally, the imputed interest is given by Eq. (41).

$$C_{\text{bat,res}} = \left(z_{\text{scr}} + (1 - z_{\text{scrap}})\; z_{\text{SOH}} \right) c_{\text{spec}}\; z_{\text{c,c2s}}\; E_{\text{bat}}\; r^{-t_{\text{own}}} \tag{39}$$

$$z_{\text{SOH}} = n_{\text{repl}} + 1 - t_{\text{own}} s_{\text{annual}} / s_{\text{life}} \tag{40}$$

$$\begin{aligned} C_{\text{bat,imp}} = & \sum_{n=0}^{n=n_{\text{repl}}-1} \frac{C_{\text{bat,inv,n}} + C_{\text{bat,scrap,n}}}{2} (r^{s_{\text{life}}/s_{\text{annual}}} - 1) \\ & + \frac{C_{\text{bat,inv,nrepl}} + C_{\text{bat,res}}}{2} (r^{(t_{\text{own}} - \frac{n_{\text{repl}}\; s_{\text{life}}}{s_{\text{annual}}})} - 1) \end{aligned} \tag{41}$$

The cost-parity price is found by using bisection to minimize the difference between the RCO of a DT and a BET.

Table 1
Analysis of cost components that differ between a BET and a DT.

Cost component	Differs between BET & DT
Powertrain	Yes
Battery	Yes
Vehicle w/o powertrain	No
Maintenance	Yes
Energy (electricity/fuel)	Yes
Taxes	Yes
Tolls	Yes
Insurance	No
Driver	No

3. Implementation

The method is demonstrated by selecting the optimal cell for a BET out of a database containing 160 unique cells. To highlight the impact of the available installed charging power, we evaluated two scenarios. In the first scenario, trucks are charged during the rest period using a 350 kW charger, which corresponds to the maximum currently available charging power under the CCS-standard [32]. In the second scenario, the trucks are charged using a 1 MW charger, which would be possible under the MCS-standard that is currently being developed for commercial vehicles and expected to be available within the next years [33]. In the following, we first present the parameters that define the use case and subsequently show the characteristics of the cells in our database.

Table 2
Use case parameters for a BET operating in Germany.

Model	Parameter	Symbol	Value		Comments & sources
Vehicle simulation	Drag area	c_A		5.68 m^2	DT Average, see Appendix B
	Rolling resistance coefficient	c_{rr}		5.48 ‰	DT Average, see Appendix B
	Engine motor power	P_{mot}		352.4 kW	DT Average, see Appendix B
	Auxiliary power consumption	P_{aux}		2.3 kW	[20] Standard trailer w/o additional auxiliaries
	Powertrain efficiency	η		85 %	[21]
	Maximum acceleration	a_{max}		1 m s^{-2}	[16]
	Deceleration	a_{dec}		1 m s^{-2}	[16]
	Gravitational acceleration	g		9.81 m s^{-2}	[16]
	Air density	ρ		1.188 kg m^{-3}	[16]
Sizing algorithm	Charging time	t_{fc}		40 min	Mandatory break period minus 5 min [17]
	Share of usable energy	z_{usable}		93 %	[22]
	Share of fast chargeable energy	z_{fc}		80 %	[10]
	Gross vehicle weight	m_{gvw}		42 t	[23]
	Vehicle weight without battery	$m_{veh,nobat}$		13.8 t	See Appendix C
	Volumetric packaging efficiency	$z_{V,c2s}$	Cylindrical	29.5 %	Electric vehicle average [24]
			Pouch/Prismatic	35.3 %	Electric vehicle average [24]
	Gravimetric packaging efficiency	$z_{m,c2s}$	Cylindrical	55.2 %	Electric vehicle average [24]
			Pouch/Prismatic	57.5 %	Electric vehicle average [24]
Cost model	Service life	t_{own}		5 years	[2]
	Annual mileage	s_{annual}		116 000 km	[18]
	Discount rate	r		1.095	[2]
	Diesel fuel cost	c_{diesel}		€1.36 L^{-1}	Average in Germany on the 1st of Jan 2022, excluding VAT
	DT consumption	b_{DT}		0.301 L km^{-1}	DT average, see Appendix B
	Battery scrappage	z_{scr}		15 %	[25]
	Cost scaling cell to system	$z_{c,c2s}$		2.07	Electric vehicle average [26]
	Share of toll kilometers	z_{toll}		92 %	[27]
	Share of fast charged energy	$z_{ene,fc}$		20 %	[2]
	Slow charging cost	c_{sc}		€0.25 kW^{-1} h	See Appendix C
	Fast charging cost	c_{fc}	350 kW	€0.29 kW^{-1} h	For a 350 kW charger in Germany on the 1st of Jan 2022, excluding VAT [28]
			1 MW	€0.37 kW^{-1} h	Limit announced by the German government [29], excluding VAT
	Maintenance costs	c_{maint}	DT	€0.147 km^{-1}	[19]
			BET	€0.098 km^{-1}	[19]
	Toll costs	c_{toll}	DT	€0.182 km^{-1}	[30]
			BET	€0 km^{-1}	[30]
	Taxes	c_{tax}	DT	€556 $years^{-1}$	[31]
			BET	€278 $years^{-1}$	[31]
	Powertrain costs	c_{pt}	DT	€48 712	See Appendix C
			BET	€34 232.51	See Appendix C

3.1. Use case

The parameters that define the use case are summarized in Table 2. To realistically model the vehicle characteristics, we used data reported for newly registered heavy-duty vehicles between the 1st January 2019 and the 30th June 2020. The analysis of the reported data and deduction of average values for a DT can be found in Appendix B. The BET was assumed to have the average drag area, tire rolling coefficient and rated engine power of the registered DTs. For the volumetric and gravimetric packaging efficiency we differentiated between cylindrical and pouch/prismatic cells. The time available for charging was assumed to be 5 min shorter than the legally required break period to account for the time it takes to connect to and disconnect from the charger. The DT fuel consumption corresponds to the reported fuel consumption at the same payload split used to determine the typical BET energy consumption. The costs for charging at 350 kW correspond to the cheapest rate in Germany [28] excl. VAT. The cost for charging at 1 MW is the upper limit for the charging cost announced by the German government [29], excl. VAT. The detailed calculations of the vehicle weight excluding the battery, the cost of slow charging and the powertrain component costs can be found in Appendix C.

3.2. Cell database

To calculate the cost-parity price, the following cell properties need to be known: energy density, specific energy, charging rate, cycle life and corresponding EOL condition. We collected these properties from publicly available cell data sheets resulting in a database containing 160 unique cells.

Since the charging rate has a large impact on the cycle life and our use case requires frequent fast charging, we used the cell charging rate at which the cycle life was specified. If the cycle life at multiple EOL conditions or charging rates was specified, we determined the cost-parity price for each configuration. Additionally, we characterized the cells according to their format and chemistry. Since the cell chemistry was mostly not specified on the data sheet, we differentiated only based on the nominal voltage: below 1.5 V as lithium-titanium-oxide (LTO) cells, between 1.5 V and 3.4 V as LFP cells, and above 3.4 V as other cell chemistries.

Fig. 4 shows the characteristics of the 160 cells in our database. The LTO cells have the lowest specific energy and energy density, followed by the LFP cells. The highest specific energy and energy densities are reached by pouch cells with a nominal voltage above 3.4 V, corresponding to 393 Wh kg^{-1} and 1047 Wh L^{-1}. The majority of cell datasheets limit charging to 1 h^{-1} or lower. The highest charging rate is provided by an LTO cell, that allows charging at 4 h^{-1}. The longest cycle life is achieved by LTO cells, followed by the LFP cells. The cylindrical cells have a shorter cycle life on average.

4. Results

The cell in our database that reaches the highest cost-parity price, meaning it can be purchased at the highest price to reach cost-parity, is

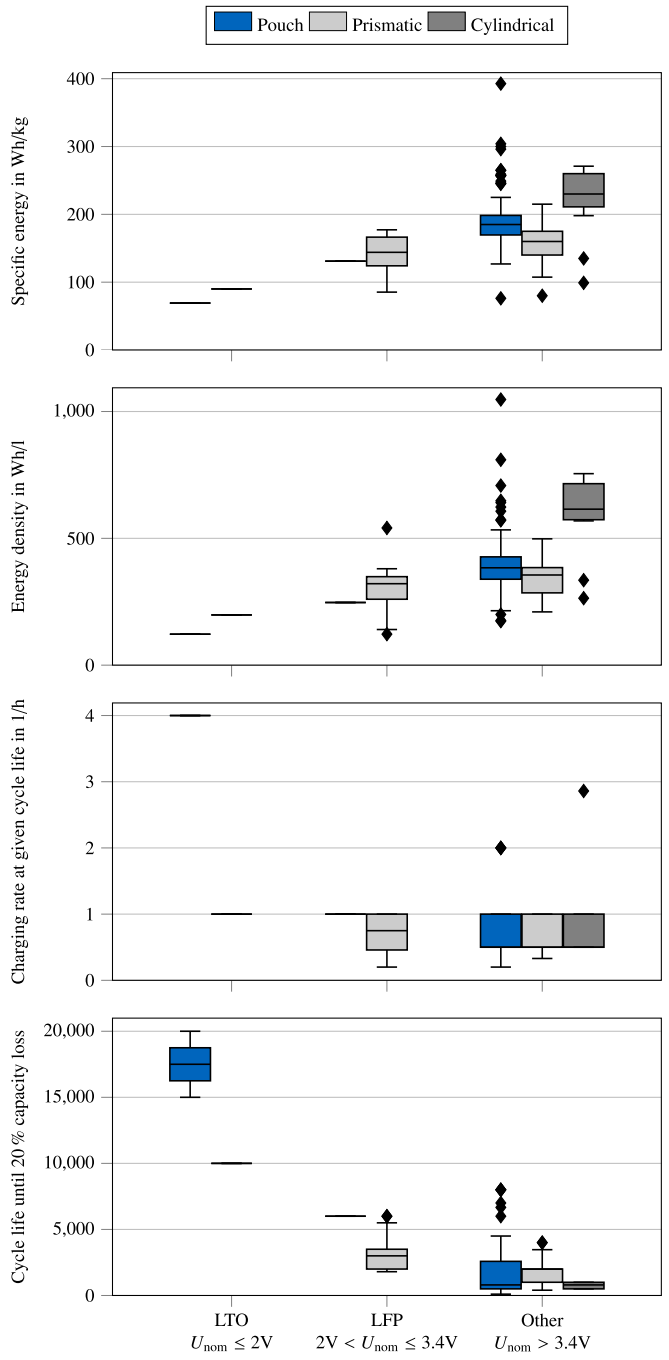

Fig. 4. Specific energy, energy density, charging rate and cycle life of the cells in our database. For the visualization, cycle life specified to different end-of-life conditions was converted to 80 % of initial capacity using cross-multiplication. In all further calculations, the specified cycle life and end-of-life condition are used.

the LG E78 in the 350 kW scenario and the Leclanché GL65 in the 1 MW scenario. In the following we will refer to these cells as reference cell 1 and 2. The reference cell properties and results from the method are summarized in Table 3.

In the following, we first illustrate the implementation of the vehicle simulation, sizing algorithm and cost model for reference cell 2 in the 1 MW charging scenario. Subsequently, the cost-parity price of all cells in our database is shown for both charging scenarios. Finally a parameter sensitivity analysis shows the impact of cell, pack, and system parameters.

Table 3
Reference cell properties and results for both charging scenarios.

Scenario	350 kW charging	1 MW charging
Capacity	78 Ah	65 Ah
Nominal voltage	3.6 V	3.72 V
Format	Pouch	Pouch
Specific energy	265 Wh kg^{-1}	216 Wh kg^{-1}
Energy density	623 Wh L^{-1}	395 Wh L^{-1}
Cycle life	1500	7000
EOL	0.8	0.8
Charging rate	0.33 h^{-1}	1 h^{-1}
Battery size	1111 kWh	792 kWh
Battery volume	5051 L	5681 L
Battery mass	7293 kg	6377 kg
Max. Payload	20.9 t	21.9 t
Typical energy consumption	1.34 kW h km^{-1}	1.32 kW h km^{-1}
Battery life	1.2×10^6 km	4.2×10^6 km
Cost-parity price	€63.12 kW^{-1} h	€96.57 kW^{-1} h

4.1. Method implementation for a single cell

Fig. 5(a) shows the result of the vehicle simulation, which is independent of the cell selection. The BET energy consumption was simulated for a range of vehicle masses, ranging from the mass of an empty vehicle excluding the battery weight up to the gross vehicle weight. Energy consumption increases with vehicle weight. The energy consumption of a fully loaded vehicle of 1.49 kW h km^{-1} matches the results from previous studies well [2,3,21,34].

Fig. 5(b) shows the battery sizing for different installed charging powers and cell charging rates. Increasing the charging rate or installed charging power reduces the required battery size because more energy can be recharged during the driver rest period. Installed charging powers above 707 kW or charging rates above 0.9 h^{-1} do not result in a further decrease of the required battery size because the battery size is limited by the energy consumption during a single leg of the trip and the share of fast-chargeable energy. The required battery size for reference cell 2 in the 1 MW charging scenario is 792 kWh.

The cost model components for the DT and BET and their differences are shown in Fig. 5(c). To reach cost-parity, the battery costs can be compensated by the lower costs of the BET in the other cost components. The costs of the powertrain, taxes, toll and maintenance are independent of the cell properties. The BET energy consumption costs depend on the battery sizing and the cell's specific mass. The battery costs are influenced by the battery sizing, cell cycle life and the cell specific cost. The cell specific cost at which cost-parity is reached, i.e. the cost-parity price, is determined using bisection. A BET using reference cell 2 in the 1 MW charging scenario would reach cost-parity with a DT if the cell can be purchased at €96.57 kW^{-1} h.

4.2. Comparison of the cells in our database

Fig. 6 shows the cost-parity price for all cells in our database versus the maximum payload and battery volume in both scenarios. The cell chemistry and format are indicated by the marker color and shape respectively. Additionally, for each scenario the reference cell is highlighted, and the reference load, maximum payload of a DT and powertrain volume of a DT are indicated.

The cost parity-price could be determined for more cells in the 1 MW charging scenario because the higher available charging power means the operating requirements can be fulfilled with a smaller battery, allowing cells with a lower specific energy to transport the reference load without exceeding the maximum payload. For the same reason, the use of reference cell 2 and LFP cells is infeasible in the 350 kW charging scenario and LTO cells cannot be used in either scenario. The smaller battery size in the 1 MW charging scenario also results in a higher cost-parity price.

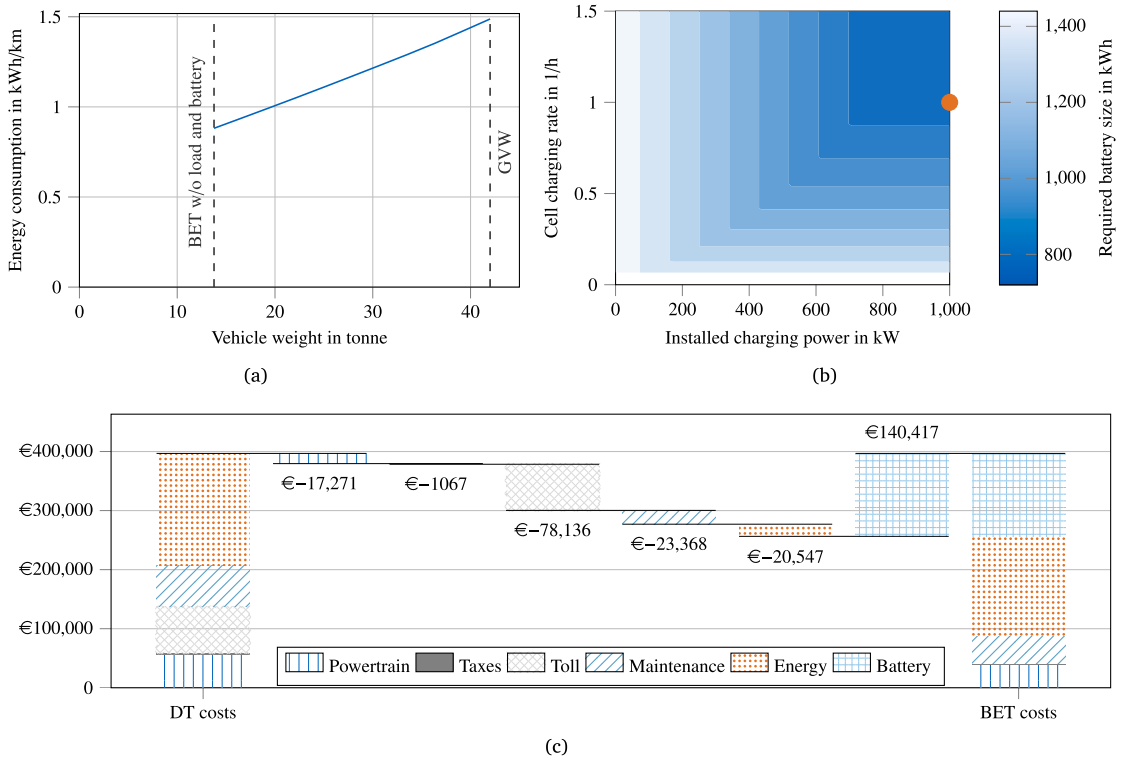

Fig. 5. Illustration of the method steps for the reference cell in the 1 MW charging scenario: (a) Vehicle energy consumption for a range of vehicle masses determined by the vehicle simulation; (b) Impact of the charging rate and installed charging power on the required battery size (marks the required battery size for reference cell 2); (c) Comparison between the DT cost components and the BET costs at a specific cell cost of €96.57 kW^{-1} h.

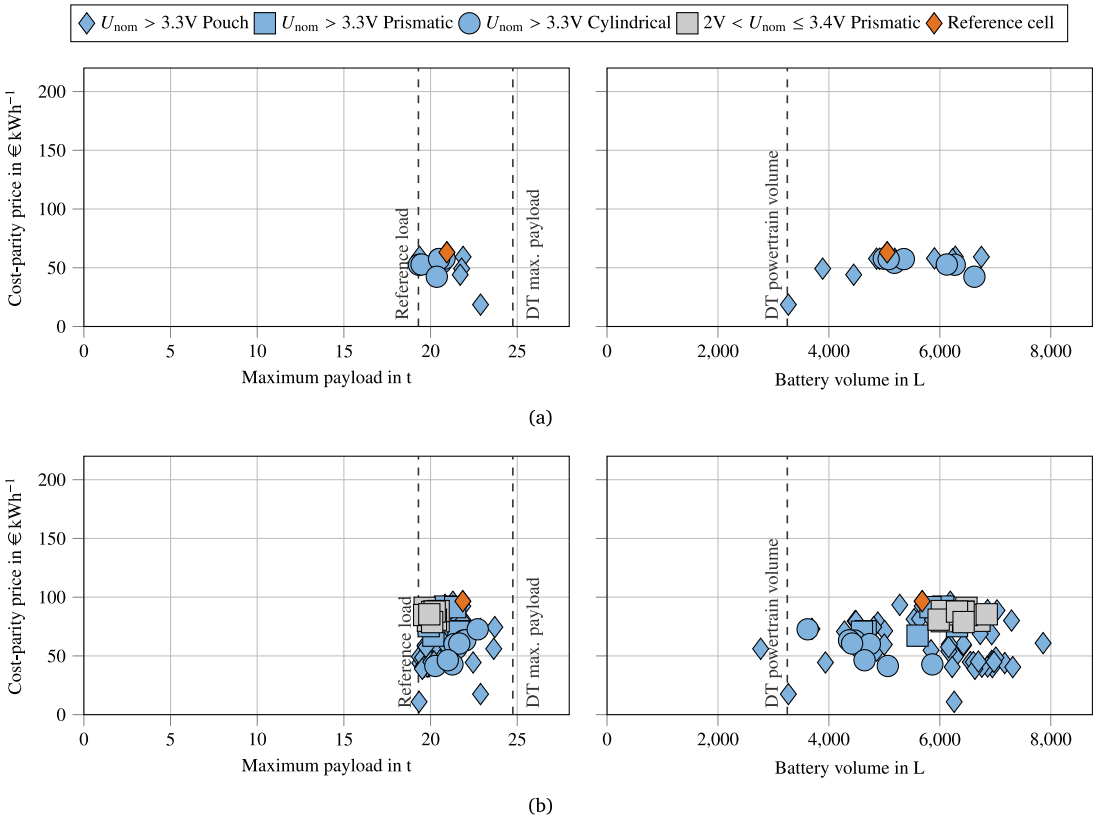

Fig. 6. Cost-parity price of all cells in the database vs. the maximum payload and required battery volume for the (a) 350 kW scenario and (b) 1 MW scenario.

The maximum payload of a DT is higher than the payload that can be realized by any cell in both scenarios. The battery volume exceeds the volume of the DT powertrain for all cells in the 350 kW scenario, whereas one cell results in a smaller battery volume in the 1 MW scenario. Vehicle manufacturers may select cells that results in a higher payload or a smaller volume than the reference cells, but would have to purchase these at a lower price to reach cost-parity with a DT, because of the lower cycle life of these cells.

4.3. Parameter sensitivity analysis

We conducted a parameter sensitivity analysis to quantify the impact of cell, pack, and system parameters on the cost-parity price, maximum payload and battery volume for reference cell 1 in the 350 kW scenario and reference cell 2 in the 1 MW scenario.

Fig. 7 shows the impact of the cell properties: cycle life, specific energy, energy density and charging rate. Each property was varied between the minimum and maximum value of all cells in our database.

The minimum and maximum cycle life of the cells in our database corresponds to 100 cycles and 20 000 cycles until 80 % of the initial capacity. Changing the cycle life does not affect the payload or required volume, but has the largest impact on the cost-parity price among the cell properties. In both charging scenarios, improving the cell's cycle life leads to a small increase in the cost-parity price, whereas reducing the cell's cycle life leads to a large reduction.

The cell's specific energy was varied between the minimum value that was able to transport the reference load, corresponding to 216 $Wh\,kg^{-1}$ and 154 $Wh\,kg^{-1}$ in the 350 kW and 1 MW charging scenarios, and the highest specific energy of a cell in our database, corresponding to 393 $Wh\,kg^{-1}$. Improving the cell's specific energy results in an increase in the cost-parity price, because the typical energy consumption is reduced. Additionally, an increase in specific energy enables a higher maximum payload. Increasing the specific energy of the reference cells to the best-in-class specific energy would enable transporting the same payload as a DT in the 1 MW charging scenario.

The cell energy density is varied between the minimum and maximum value of the cells in our database, corresponding to 122 $Wh\,L^{-1}$ and 1047 $Wh\,L^{-1}$. The cell energy density only affects the battery volume and is therefore only shown in the right panes of Fig. 7. The lower energy density limit results in a battery volume exceeding the figure bounds and is therefore indicated by an arrow. The best-in-class energy density would result in a smaller battery volume than the volume that would become available if the DT powertrain is removed.

Finally, the impact of the cell's charging rate is shown. Increasing the charging rate beyond 0.3 h^{-1} in the 350 kW charging scenario and 0.9 h^{-1} in the 1 MW charging scenario does not reduce the required battery size, as was shown in Fig. 5(b). In the 1 MW charging scenario, the lower limit is the minimum value that enables transporting the reference load. Increasing the charging rate leads to an increase in cost-parity-price and maximum payload, and a decrease of the battery volume, because the required battery size is decreased.

Fig. 8 shows the impact of the pack parameters: the cell-to-pack cost ratio, gravimetric packaging efficiency and volumetric packaging efficiency. The cell-to-pack cost ratio was varied between the minimum and maximum values reported for battery-electric vehicles in the year 2020 by König et al. [26], corresponding to 1.94 and 2.21. Reducing the cell-to-pack cost ratio results in a higher cost-parity price, while it does not affect the maximum payload or battery volume.

The gravimetric packaging efficiency was varied between the minimum and maximum value for pouch cells in commercial battery-electric vehicles [24], corresponding to 49.5 % and 74.2 %. Increasing the gravimetric packaging efficiency results in a higher cost-parity

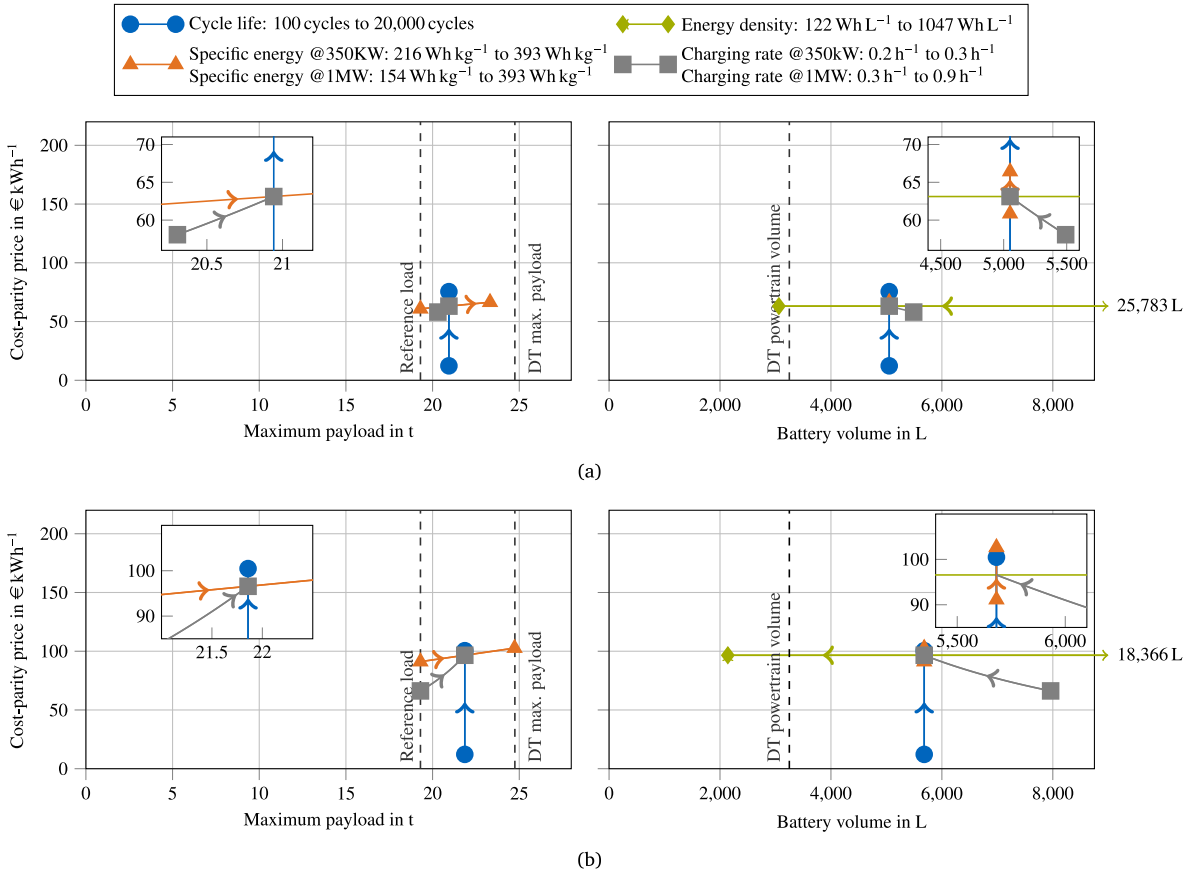

Fig. 7. Impact of cell properties on the cost-parity price, maximum payload and battery volume for (a) the 350 kW scenario and (b) the 1 MW scenario. The insets show a close-up of the area around the reference cell characteristics. The arrow indicates the direction of the parameter variation.

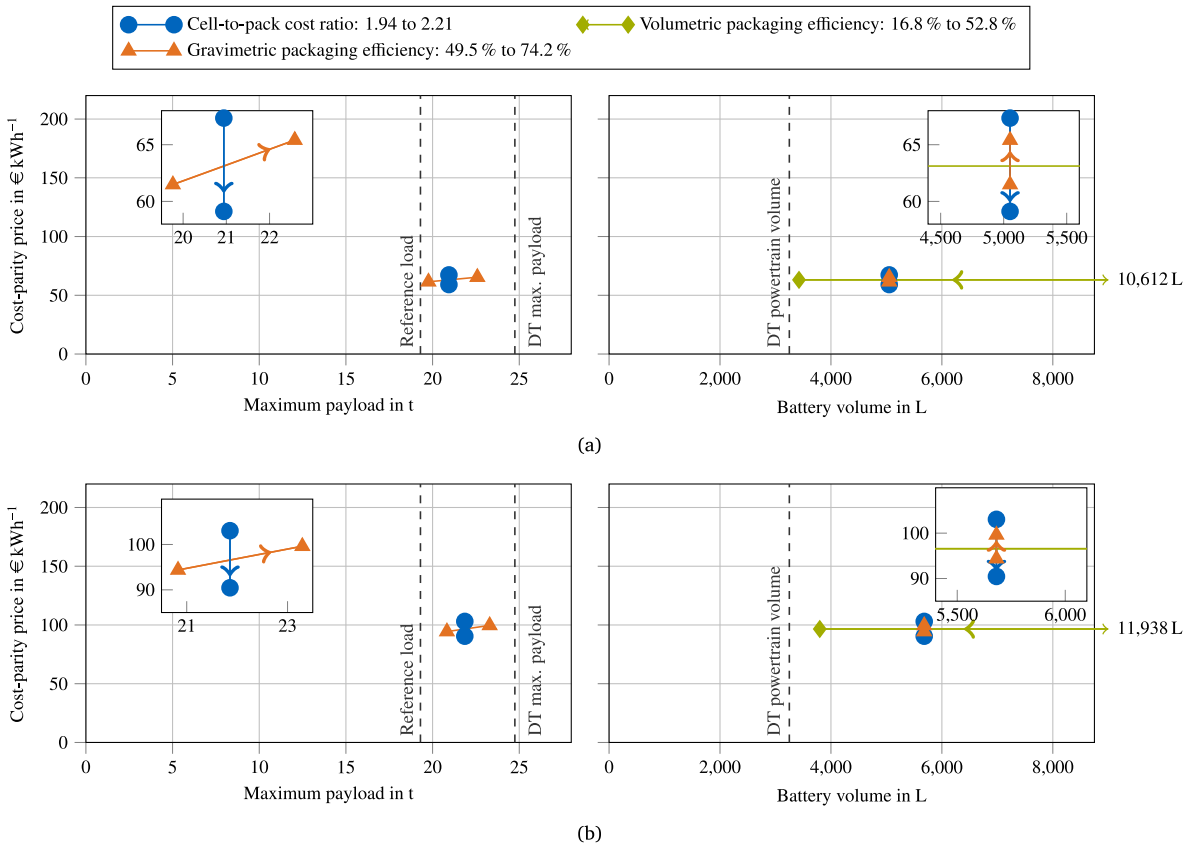

Fig. 8. Impact of pack properties on the cost-parity price, maximum payload and battery volume for (a) the 350 kW scenario and (b) the 1 MW scenario. The insets show a close-up of the area around the reference cell characteristics. The arrow indicates the direction of the parameter variation.

price, since the typical energy consumption is decreased. Additionally, the maximum payload is increased. However, even at the best-in-class gravimetric packaging efficiency, the reference cells do not achieve the same payload as a DT in either scenario.

The volumetric packaging efficiency was varied between 16.8 % and 52.8 %, corresponding to the minimum and maximum values for pouch cells used in commercial battery-electric vehicles [24]. The volumetric packaging efficiency only affects the battery volume and is therefore only shown in the right panes of Fig. 8. The lower limit requires a volume exceeding the figure bounds and is therefore indicated by an arrow. Increasing the volumetric packaging efficiency results in a smaller battery volume, but even the best-in-class packaging efficiency results in a battery with more volume than the DT powertrain.

Fig. 9 shows the impact of the system parameters: annual mileage, service life, diesel cost, cost of charging, and vehicle energy consumption. Apart from the vehicle energy consumption, the system parameters only influence the cost-parity price and not the payload or battery volume.

For the annual mileage, the lower limit corresponds to the average annual mileage of all semi-trailer trucks in Germany, including drayage trucks [35]. The upper limit is the annual mileage resulting from driving 9 h a day on 250 days a year. On the one hand, increasing the annual mileage reduces the battery residual value at the end of the service life. On the other hand, BETs benefit from a lower cost per kilometer than DTs for toll, maintenance and energy costs. Overall, the latter effect is more significant, which results in an increased cost-parity price as the annual mileage increases.

For the BET energy consumption, the lower limit corresponds to the typical and maximum energy consumption simulated for a truck with the lowest reported rolling friction coefficient and drag area of all trucks registered between the 1st January 2019 and the 30th June 2020. The upper limit corresponds to the values that were used in the case study, as defined in Table 2. Reducing the energy consumption results in an increase in the cost-parity price, since the required battery size is reduced and the typical energy consumption is decreased. Additionally, reducing energy consumption results in a higher maximum payload and smaller battery volume.

For the service life, the lower limit corresponds to the payback period considered by large fleets [36] and the upper limit is the average service life of a truck in Germany [5]. The cost-parity price decreases as the service life is increased, because a longer service life results in a longer bound investment and a smaller net present value of the residual battery value.

The cost of charging is varied between the cost that might be realized if truck companies can participate in the electricity wholesale market [34] and the current upper limit for the charging cost stipulated by the German government, excluding VAT. [29]. Increasing the cost of charging results in a decrease in the cost-parity price.

Finally, the diesel cost is varied between the lowest and highest diesel cost in Germany excluding VAT between Jan 2021 and March 2022 [37]. An increase in the diesel cost results in an increase in the cost-parity price.

Comparing the impact of cell-, pack, and system parameters shows that improving the cell specific energy and energy density has the biggest impact on matching the payload and volume of a DT powertrain. This can be supported by improving the volumetric and gravimetric packaging efficiencies. The impact of improving the cycle life beyond the cycle life of the reference cells is relatively small, but reducing the cycle life leads to a strong decline in the cost-parity price. The biggest potential to increase the cost-parity price is providing 1 MW charging, reducing the cost of charging and reducing the vehicle energy consumption.

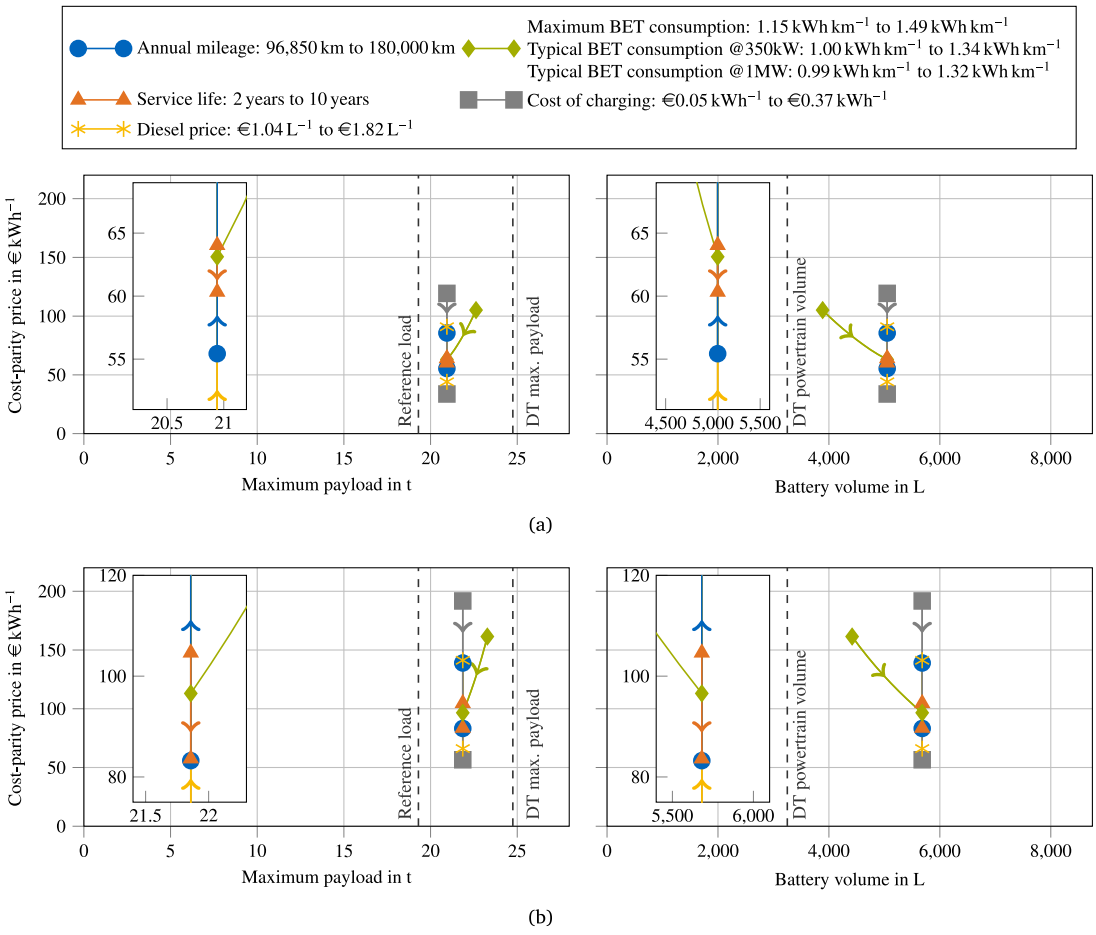

Fig. 9. Impact of system properties on the cost-parity price, maximum payload and battery volume for (a) the 350 kW scenario and (b) the 1 MW scenario. The insets show a close-up of the area around the reference cell characteristics. The arrow indicates the direction of the parameter variation.

5. Discussion

Techno-economic cell-selection extends traditional cell selection methods, such as the Ragone plot, by quantifying the impact of individual cell characteristics on the system cost. The visualization in Fig. 6 allows truck manufacturers to compare the cost-parity price of different cells with properties that do not influence the system cost directly, such as the maximum payload and battery volume. Based on this visualization, a truck manufacturer can exclude cells that do not meet the payload and volume requirements for a given vehicle concept. Additionally, cells that are not available in the required quantities or that do not meet safety standards can be excluded. Other constraints, such as the preferred cell format, or a minimum cell capacity for handling during production may be considered. By obtaining quotes for the remaining cells, and comparing these to the cost-parity price for each cell, the optimal cell can be selected. Additionally, the parameter sensitivity analysis of the pack and system parameters, and the comparison of different scenarios show how system performance can be improved independent from the cell selection.

Techno-economic cell selection is not only suitable for helping truck manufacturers to select the optimal cell, but also provides cell manufacturers with insights. First, the cost-parity price quantifies at which price point a cell becomes cost-competitive. Second, the parameter sensitivity analysis, illustrated in Fig. 7, shows which price increases are justified if individual cell properties are improved. Finally, the sensitivity analysis of use case parameters and the comparison of different scenarios can support the anticipation of future business opportunities for cell technologies.

Techno-economic cell selection relies solely on values provided in cell data sheets. This enables the comparison of a wide range of different cells during the early-stage design phase before conducting resource-intensive parametrization studies. However, this approach also leads to simplifications. Most notably, the data provided on the cell's aging behavior is limited. Only cyclic battery aging can be considered, since data sheets do not provide information on the storage life of a cell. Furthermore, due to the limited information available in cell datasheets, the impact of the depth of discharge, C-rate, and temperature on the battery life cannot be quantified. Therefore, after using the method to shortlist one or multiple cells, a detailed characterization of the electric, thermal and aging behavior of the cell is required to estimate the battery life for the given usage condition and optimize further design parameters such as the battery size or the battery thermal management system.

We demonstrated techno-economic cell-selection by selecting a cell from a database containing 160 unique cells for a long-haul truck operating with a single driver in Germany. The results show that for BETs charged at 350 kW, the cell price needs to drop to ca. €60 kW^{-1} h to reach cost-parity with a DT. When 1 MW charging power is available, cost-parity can be reached at a cell price around €100 kW^{-1} h, which is within reach of optimistic cost estimates [26]. The maximum payload of a BET charged with 1 MW using reference cell 2 would be 2.9 t less than a DT, which may be acceptable because trucks are mostly volume-constrained instead of payload-constrained [8]. The required volume, however, would be almost double the volume of the DT powertrain, which may be challenging to realize. Other cells provide a higher maximum payload and require less volume, but need to be purchased at a lower price to reach cost-parity, due to their lower cycle life.

The parameter sensitivity analysis showed that improving packaging efficiency and vehicle energy consumption can support matching the payload and powertrain volume of a diesel truck, while the cost of charging and vehicle energy consumption provide the biggest opportunity for increasing the cost-parity price. These results indicate that it will remain challenging, but possible, to make BETs cost-competitive with DT.

For our use case, we sized the battery based on the single-driver daily driving-time limit of 10 h and an average speed of 80 $km\,h^{-1}$, which results in a maximum daily driving distance of 800 km. This approach covers a large share of truck driving patterns: Basma et al. [2] and Tol et al. [38] show that 98 % of truck daily distances in Europe are shorter than 800 km, where the remaining 2 % are likely operated by multiple drivers. That said, trip distances and durations vary widely. Link et al. [39] recorded over one million vehicle kilometers from a German truck fleet revealing high variance in durations and distances of single trips, daily mileage, number of trips per day, and different shift schedules (i.e., single shift or multi-shift operations). Similarly, Tol et al. [38] find a standard deviation of up to 40% for day-to-day distances for current DT. This indicates the potential of an individual battery sizing and highlights the importance of future research in truck travel patterns.

Furthermore, we assumed that a charger is available after 4.5 h of driving, resulting in a maximum distance between two chargers of 360 km. This is in-line with the targets of the European Commission for electric recharging infrastructure dedicated to heavy-duty vehicles [40]: By the end of 2025 a 350 kW charger shall be available every 60 km along the TEN-T-core network and every 100 km along the TEN-T-comprehensive network. However, the MCS-Standard that will enable 1 MW charging will only be available from the mid-2020s, and in addition to charging infrastructure at public rest areas, semi-public charging infrastructure needs to be available to enable trucks to charge while loading and unloading cargo [39]. The presented results are therefore only valid, if the available charging infrastructure is increased and future research in charging infrastructure optimization is required.

Finally, although we took great care in using realistic design criteria and use case parameters for the BET application, the following limitations should be taken into account. First, our cell database contains information from data sheets that were available to researchers, which might not reflect the status quo of cells used in the automotive industry [41]. Second, operation with multiple drivers, or with cooled trailers would influence the battery sizing. Third, the cost function assumes a linear depreciation of the battery value with the vehicle mileage, favoring cells with a high cycle life. However, it might not be in the interest of vehicle manufacturers to provide a battery life that exceeds the warranty conditions. Fourth, the impact of axle load limitations on the battery sizing should be considered before selecting a cell. Finally, the results are specific to a truck operating in Germany today. Policy measures, such as toll and tax exemptions, the cost of charging and diesel cost vary widely in different countries and have a large impact on the cost-competitiveness of BET [2,6]. By publishing the source code of our method, we hope to enable other researchers to extend the cell database, sizing model and cost model, and implement the techno-economic cell selection in further scenarios.

6. Conclusion

Techno-economic cell selection is a novel cell selection method that takes the trade-off between cost and performance into consideration. Additionally, the method enables quantifying the impact of improving cell, pack, and system properties. We demonstrated the method by selecting a cell from a database containing 160 unique cells for a long-haul truck operating with a single driver in Germany. Our results show that, when 1 MW charging is available, the best performing cell becomes cost-competitive around €100 kW^{-1} h, which is within reach of price estimates for lithium-ion cells today. However, the achievable payload and required volume on board the vehicle still pose challenges for battery technology.

In future work, we plan to implement techno-economic cell selection in further automotive and non-automotive applications to show the general applicability and compare cost-parity prices across applications.

CRediT authorship contribution statement

Olaf Teichert: Conceptualization, Methodology, Software, Writing – original draft. **Steffen Link:** Methodology, Investigation, Data curation, Writing – original draft. **Jakob Schneider:** Investigation, Writing – review & editing. **Sebastian Wolff:** Validation, Writing – review & editing. **Markus Lienkamp:** Resources, Supervision, Writing – review & editing, Funding acquisition.

Declaration of competing interest

The authors declare that they have no known competing financial interests or personal relationships that could have appeared to influence the work reported in this paper.

Data availability

Data will be made available on request.

Acknowledgments

The work of O.T. and S.L. was sponsored by the Federal Ministry of Education and Research Germany with the project “BetterBat” under grant number 03XP0362C. The work of J.S. was sponsored by the Federal Ministry for Economic Affairs and Energy Germany within the project “NEFTON” under grant number 01MV21004A. The work of S.W. was funded by general research funds of the Technical University of Munich, Germany. We would like to thank M.(anuel) Bstieler for preparing the visualization of a DT during his student thesis.

Appendix A. Battery energy throughput for different charging scenarios

Fig. A.1 illustrates the cumulative energy throughput of a truck battery for two scenarios: with a 350 kW and 1 MW charger available during the rest period. In both scenarios the truck consumes 530 kWh of energy during the driving phase, but due to the different charging powers, the cumulative energy throughput after the second driving event is larger for the 350 kW charging scenario. Further reductions in the amount of recharged energy may be caused by the cell’s maximum charging rate. Note that the amount of fast chargeable energy during the rest period is limited to 80 % of the usable energy at the end of life of the battery. As a result, in the 1 MW scenario the battery is fully recharged before the end of the rest period, which shows that a lower charging power would have been sufficient. The required battery size

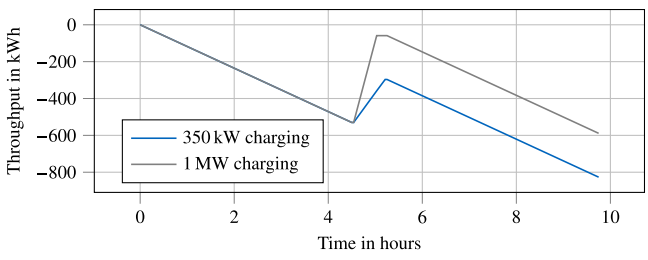

Fig. A.1. Energy throughput of a battery charged with 350 kW and 1 MW during the charging break.

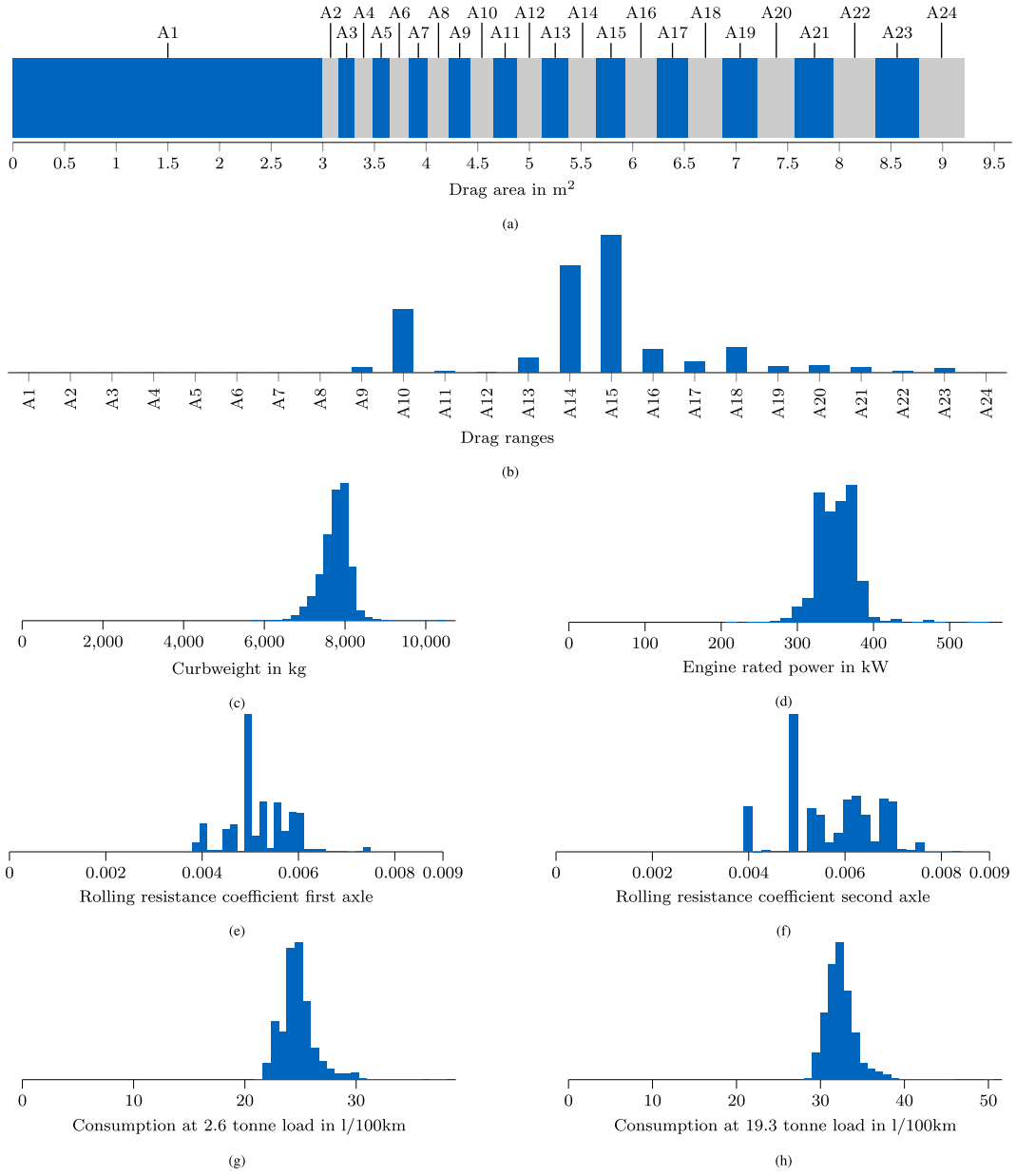

Fig. B.1. (a) Drag ranges defined by the European Parliament and the council [42]; (b-h) reported vehicle characteristics of 161 129 trucks in the vehicle sub-group "LH-5" that were registered between the 1st January 2019 and the 30 June 2020.

is determined by dividing the cumulative energy throughput after the second driving event by the EOL condition and the share of usable energy. If the amount of rechargeable energy is not limited by the cell's charging rate, the required battery size for the 350 kW and 1 MW charging scenario are 792 kWh and 1111 kWh respectively.

Appendix B. Analysis of reported long-haul truck data

To realistically model the vehicle characteristics, we use data that heavy-duty vehicle manufacturers are required to report in accordance with EU Regulation 2018/956. We limit the data to vehicle sub-group "LH-5", which comprises tractors that have a 4 × 2 axle configuration, a sleeper cab, and a technically permissible maximum laden mass over 16 tonnes [18]. This vehicle sub-group makes up 62 % of new regulated truck sales [43]. The parameters of interest for the vehicle simulation are the engine rated power, drag area, and tire rolling resistance coefficient. Additionally, the chassis curb mass is required to determine the vehicle mass for the sizing algorithm, and the consumption of a diesel truck is needed for the cost model.

The reported data directly includes the chassis curb mass and the engine rated power. The rolling resistance coefficient is given for the first and second axle, the fuel consumption is specified for a 2.6 t and 19.3 t load and the drag area is specified according to the drag ranges defined by the European Commission, shown in Fig. B.1(a). The distribution of these parameters for 161 129 trucks registered between the 1st of January 2019 and the 30th June 2020 is shown in Fig. B.1(b) to B.1(h).

The average values are summarized in Table B.1. For the rolling resistance coefficient this is the average of the front and rear axle. The drag area is calculated by assuming that the center of each drag range is representative for the drag areas in that range. The average diesel truck fuel consumption is determined based on the loading conditions defined by the European Commission, which correspond to 2.6 t over 30 % of the trip distance and 19.3 t over the remaining 70 %.

Table B.1
Average vehicle parameters of 161,129 trucks in the vehicle sub-group "LH-5" that were registered between the 1st January 2019 and the 30 June 2020.

Parameter	Average
Engine rated power	352.4 kW
Rolling resistance coefficient	0.00548
Drag area	5.68 m^2
Chassis curb mass	7753 kg
DT fuel consumption	0.301 L km^{-1}

Appendix C. Vehicle weight without battery, cost of slow charging and powertrain component costs

The vehicle weight without the battery is the sum of the average DT chassis curb mass (7753 kg, Table B.1), minus the weight of the DT powertrain (25 % [44]), plus the weight of the e-axle (450 kg [8]), plus the weight of the trailer (7500 kg [45]), resulting in 13.8 t.

The costs of slow charging corresponds to the sum of the average industrial electricity price in 2021 of €0.2138 kW^{-1} h [46] and an overhead costs for the overnight charging infrastructure of €0.0377 kW^{-1} h [2]. The resulting cost of slow charging is €0.2515 kW^{-1} h.

We model the powertrain costs based on the specific direct manufacturing costs for major powertrain components in the reference year 2020 published by Speth et al. [47]. For DT, these are the internal combustion engine plus gearbox (€72 kW^{-1}), fuel tank (€2 L^{-1}, 800 L tank volume), and the emission after-treatment system (€19.8 kW^{-1}). For BETs, these are electric motors (€32 kW^{-1}) and power electronics plus HV system components (€35 kW^{-1}). Additionally, we use a markup factor of 1.45 to account for indirect manufacturing costs such as overhead, warranty and margins [2]. The resulting powertrain costs for the DT and BET are €49 223.64 and €34 232.51 respectively.

Appendix D. DT powertrain volume

The powertrain volume of a DT is determined using a package model of a diesel 4 × 2 semi-tractor with a wheelbase of 3600 mm, as shown in Fig. D.1(a). When converting the DT to a BET, the cab, frame, wheelbase, and axles remain unchanged [48]. By removing all ICEV-specific components (engine, tank, transmission, cardan shaft, exhaust), large areas outside the ladder frame (between the axles) and in the engine compartment are freed up, as illustrated in Fig. D.1(b). The total volume that becomes available is 3250 L. Smaller, irregular areas and the inside of the ladder frame at the rear axle, which is reserved for the axle suspension and the electric motor [49] are not included.

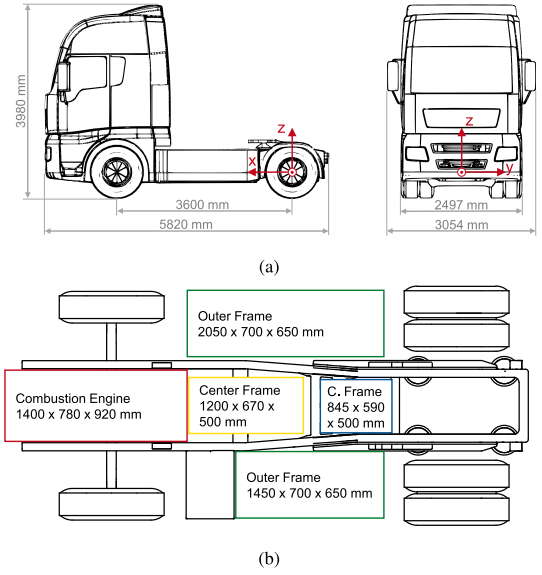

Fig. D.1. Visualization of (a) the DT measurements, and (b) the volume that becomes available when the DT powertrain components are removed.

References

[1] Meszler D, Delgado O, Rodríguez F, Muncrief R. European heavy-duty vehicles: Cost-effectiveness of fuel-efficiency technologies for long-haul tractor-trailers in the 2025–2030 timeframe. International Council on Clean Transportation; 2018, www.theicct.org/publications/cost-effectiveness-of-fuel-efficiency-tech-tractor-trailers.

[2] Basma H, Saboori A, Rodríguez F. Total cost of ownership for tractor-trailers in Europe: Battery electric versus diesel. International Council on Clean Transportation; 2021, https://theicct.org/sites/default/files/publications/TCO-BETs-Europe-white-paper-v4-nov21.pdf.

[3] Sripad S, Viswanathan V. Quantifying the economic case for electric semi-trucks. ACS Energy Lett 2018;4(1):149–55. http://dx.doi.org/10.1021/acsenergylett.8b02146.

[4] Forrest K, Mac Kinnon M, Tarroja B, Samuelsen S. Estimating the technical feasibility of fuel cell and battery electric vehicles for the medium and heavy duty sectors in California. Appl Energy 2020;276:115439. http://dx.doi.org/10.1016/j.apenergy.2020.115439.

[5] Wolff S, Lienkamp M, Schaller K-V. Status nutzfahrzeuge 2020: Alles auf eine karte? Researchgate; 2021.

[6] Noll B, del Val S, Schmidt TS, Steffen B. Analyzing the competitiveness of low-carbon drive-technologies in road-freight: A total cost of ownership analysis in Europe. Appl Energy 2022;306:118079. http://dx.doi.org/10.1016/j.apenergy.2021.118079.

[7] Sripad S, Viswanathan V. Performance metrics required of next-generation batteries to make a practical electric semi truck. ACS Energy Lett 2017;2(7):1669–73. http://dx.doi.org/10.1021/acsenergylett.7b00432.

[8] Mareev I, Becker J, Sauer DU. Battery dimensioning and life cycle costs analysis for a heavy-duty truck considering the requirements of long-haul transportation. Energies 2018;11(1):55. http://dx.doi.org/10.3390/en11010055.

[9] Çabukoglu E, Georges G, Küng L, Pareschi G, Boulouchos K. Battery electric propulsion: An option for heavy-duty vehicles? Results from a Swiss case-study. Transp Res C 2018;88:107–23. http://dx.doi.org/10.1016/j.trc.2018.01.013.

[10] Nykvist B, Olsson O. The feasibility of heavy battery electric trucks. Joule 2021;5(4):901–13. http://dx.doi.org/10.1016/j.joule.2021.03.007.

[11] Mauler L, Dahrendorf L, Duffner F, Winter M, Leker J. Cost-effective technology choice in a decarbonized and diversified long-haul truck transportation sector: A US case study. J Energy Storage 2022;46:103891. http://dx.doi.org/10.1016/j.est.2021.103891.

[12] Ragone DV. Review of battery systems for electrically powered vehicles. In: Proceedings of the Society of Automotive Engineers Mid-Year Meeting, Detroit, Michigan, May 20-24. 1968, http://dx.doi.org/10.4271/680453.

[13] Christen T, Carlen MW. Theory of Ragone plots. J Power Sources 2000;91(2):210–6. http://dx.doi.org/10.1016/S0378-7753(00)00474-2.

[14] Catenaro E, Rizzo DM, Onori S. Experimental analysis and analytical modeling of enhanced-Ragone plot. Appl Energy 2021;291:116473. http://dx.doi.org/10.1016/j.apenergy.2021.116473.

[15] Dechent P, Epp A, Jöst D, Preger Y, Attia PM, Li W, et al. ENPOLITE: Comparing lithium-ion cells across energy, power, lifetime, and temperature. ACS Energy Lett 2021;6:2351–5. http://dx.doi.org/10.1021/acsenergylett.1c00743.

[16] European Commission. User Manual: Vehicle energy consumption calculation tool. 2023.

[17] The European parliament and the council. The harmonisation of certain social legislation relating to road transport and amending council regulations (EEC) No 3821/85 and (EC) No 2135/98 and repealing council regulation (EEC) No 3820/85. 2006, https://eur-lex.europa.eu/eli/reg/2006/561/oj.

[18] The European Parliament and The Council. Regulation (EU) 2019/1242: Setting CO2 emission performance standards for new heavy-duty vehicles and amending regulations (EC) No 595/2009 and (EU) 2018/956 of the European Parliament and of the Council and Council Directive 96/53/EC. 2019, https://eur-lex.europa.eu/eli/reg/2019/1242/oj.

[19] Kleiner F, Friedrich HE. Maintenance & repair cost calculation and assessment of resale value for different alternative commercial vehicle powertrain technologies. In: Proceedings of the 30th Electric Vehicle Symposium. 2017, https://elib.dlr.de/114666/.

[20] Zhao H, Burke A, Miller M. Analysis of class 8 truck technologies for their fuel savings and economics. Transp Res Part D: Transp Environ 2013;23:55–63. http://dx.doi.org/10.1016/j.trd.2013.04.004.

[21] Earl T, Mathieu L, Cornelis S, Kenny S, Ambel CC, Nix J. Analysis of long haul battery electric trucks in EU. Transport & Environment; 2018, https://www.transportenvironment.org/discover/analysis-long-haul-battery-electric-trucks-eu/.

[22] Wassiliadis N, Steinsträter M, Schreiber M, Rosner P, Nicoletti L, Schmid F, et al. Quantifying the state of the art of electric powertrains in battery electric vehicles: Range, efficiency, and lifetime from component to system level of the Volkswagen ID. 3. ETransportation 2022;12:100167. http://dx.doi.org/10.1016/j.etran.2022.100167.

[23] Bundesministerium der Justiz. Straßenverkehrs-zulassungs-ordnung §34. 2002, http://www.gesetze-im-internet.de/stvzo_2012/__34.html.

[24] Löbberding H, Wessel S, Offermanns C, Kehrer M, Rother J, Heimes H, et al. From cell to battery system in BEVs: Analysis of system packing efficiency and cell types. World Electr Veh J 2020;11(4):77. http://dx.doi.org/10.3390/wevj11040077.

[25] Burke A, Fulton L. Analysis of advanced battery-electric long haul trucks: Batteries, performance, and economics. UC Davis Institute of Transportation Studies; 2019, https://ucdavis.app.box.com/s/cfpoywahc2so21hogykiga6h8r9rppxe.

[26] König A, Nicoletti L, Schröder D, Wolff S, Waclaw A, Lienkamp M. An overview of parameter and cost for battery electric vehicles. World Electr Veh J 2021;12(1):21. http://dx.doi.org/10.3390/wevj12010021.

[27] Hülsmann F, Mottschall M, Hacker F, Kasten P. Konventionelle und alternative fahrzeugtechnologien bei pkw und schweren nutzfahrzeugen - potenziale zur minderung des energieverbrauchs bis 2050. Öko-Institut; 2014, https://digital.zlb.de/viewer/metadata/15823045/1/.

[28] Ionity. Access and payment, ionity-passport. 2022, https://ionity.eu/en/access-and-payment.html, [Accessed 14 February 2022].

[29] NOW-GmbH. Deutschlandnetz: Bundesverkehrsminister scheuer stellt 1.000 standorte für schnellladesäulen und preismodell vor. 2021, https://www.now-gmbh.de/aktuelles/pressemitteilungen/deutschlandnetz-bundesverkehrsminister-scheuer-stellt-1-000-standorte-fuer-schnellladesaeulen-und-preismodell-vor/. [Accessed 09 February 2022].

[30] Bundesministerium der Justiz. Gesetz über die erhebung von streckenbezogenen gebühren für die benutzung von bundesautobahnen und bundesstraßen §1. 2011, https://www.gesetze-im-internet.de/bfstrmg/__1.html.

[31] Bundesministerium der Justiz. Kraftfahrzeugsteuergesetz §9. 2002, https://www.gesetze-im-internet.de/kraftstg/__9.html.

[32] Coordination Office Charging Interface. Combined Charging system 1.0 specification - CCS 1.0. Version 1.2.1.

[33] CHARIN. Megawatt charging system (MCS). 2022, https://www.charin.global/technology/mcs/. [Accessed on 28 April 2022].

[34] Phadke A, McCall M, Rajagopal D. Reforming electricity rates to enable economically competitive electric trucking. Environ Res Lett 2019;14(12):124047. http://dx.doi.org/10.1088/1748-9326/ab560d.

[35] Kraftfahrtbundesamt. Verkehr in kilometern 1.25 sattelzugmaschinen nach fahrzeugalter seit 2014. 2020, https://www.kba.de/DE/Statistik/Produktkatalog/produkte/Kraftverkehr/vk_uebersicht.html.

[36] The future of trucks - implications for energy and the environment. International Energy Agency; 2017, http://dx.doi.org/10.1787/9789264279452-en.

[37] ADAC. Kraftstoffpreisentwicklung. 2022, https://www.adac.de/verkehr/tanken-kraftstoff-antrieb/deutschland/kraftstoffpreisentwicklung/. [Accessed 19 April 2022].

[38] Tol D, Frateur T, Verbeek M, Riemersma I, Mulder H. Techno-economic uptake potential of zero-emission trucks in Europe. TNO; 2022.

[39] Link S, Plötz P, Griener J, Moll C. Lieferverkehr mit batterie-lkw: Machbarkeit 2021. Fraunhofer-Institut für System- und Innovationsforschung ISI; 2021, http://dx.doi.org/10.24406/publica-fhg-301266.

[40] The European parliament and the council. Proposal for a regulation on the deployment of alternative fuels infrastructure, and repealing directive 2014/94/EU of the European Parliament and of the Council. 2021, https://eur-lex.europa.eu/legal-content/en/TXT/?uri=CELEX:52021PC0559.

[41] Teichert O, Grube Doiz N, Schreiber M, Lin X, Lienkamp M. Substandard? Lithium-ion cells available on online marketplaces. In: Advanced battery power. 2022, http://dx.doi.org/10.13140/RG.2.2.19218.12480.

[42] The European Parliament and The Council. Regulation (EU) 2018/956: On the monitoring and reporting of CO2 emissions from and fuel consumption of new heavy-duty vehicles. 2018, https://eur-lex.europa.eu/legal-content/EN/TXT/?uri=celex:32018R0956.

[43] Ragon P-L, Rodríguez F. CO2 emissions from trucks in the EU: An analysis of the heavy-duty CO2 standards baseline data. The International Council on Clean Transportation; 2021, https://theicct.org/publication/co2-emissions-from-trucks-in-the-eu-an-analysis-of-the-heavy-duty-co2-standards-baseline-data/.

[44] Phadke A, Khandekar A, Abhyankar N, Wooley D, Rajagopal D. Why regional and Long-Haul trucks are primed for electrification now. Lawrence Berkeley National Laboratory; 2021, https://escholarship.org/uc/item/3kj8s12f.

[45] Norris J, Escher G. Heavy duty vehicles technology potential and cost study. The International Council on Clean Transportation; 2017, https://theicct.org/publication/heavy-duty-vehicles-technology-potential-and-cost-study/.

[46] BDEW. Strompreisanalyse Juni 2021. 2021, https://www.bdew.de/service/daten-und-grafiken/bdew-strompreisanalyse/. [Accessed 27 April 2022].

[47] Speth D, Kappler L, Link S, Keller M. Attractiveness of alternative fuel trucks with regard to current tax and incentive schemes in Germany: A total cost of ownership analysis. In: Proceedings of the 35th Electric Vehicle Symposium. 2022, http://dx.doi.org/10.24406/publica-228.

[48] Wolff S, Seidenfus M, Gordon K, Álvarez S, Kalt S, Lienkamp M. Scalable life-cycle inventory for heavy-duty vehicle production. Sustainability 2020;12(13):5396. http://dx.doi.org/10.3390/su12135396.

[49] Wolff S, Kalt S, Bstieler M, Lienkamp M. Influence of powertrain topology and electric machine design on efficiency of battery electric trucks—A simulative case-study. Energies 2021;14(2):328. http://dx.doi.org/10.3390/en14020328.